

**Atomic-Scale Measurement of Flexoelectric Polarization at SrTiO<sub>3</sub> Dislocations**Peng Gao,<sup>1,2,3,4,\*‡</sup> Shuzhen Yang,<sup>5,‡</sup> Ryo Ishikawa,<sup>1</sup> Ning Li,<sup>2</sup> Bin Feng,<sup>1</sup> Akihito Kumamoto,<sup>1</sup> Naoya Shibata,<sup>1</sup> Pu Yu,<sup>4,5</sup> and Yuichi Ikuhara<sup>1,6,7,†</sup><sup>1</sup>*Institute of Engineering Innovation, School of Engineering, The University of Tokyo, Tokyo 113-8656, Japan*<sup>2</sup>*International Center for Quantum Materials, School of Physics, Peking University, Beijing 100871, China*<sup>3</sup>*Electron Microscopy Laboratory, School of Physics, Peking University, Beijing 100871, China*<sup>4</sup>*Collaborative Innovation Center of Quantum Matter, Beijing 100871, China*<sup>5</sup>*State Key Laboratory of Low Dimensional Quantum Physics and Department of Physics, Tsinghua University, Beijing 100084, China*<sup>6</sup>*Nanostructures Research Laboratory, Japan Fine Ceramic Center, Nagoya 456-8587, Japan*<sup>7</sup>*WPI Advanced Institute for Materials Research, Tohoku University, Sendai 980-8577, Japan*

(Received 7 March 2018; revised manuscript received 6 May 2018; published 29 June 2018)

Owing to the broken translational symmetry at dislocations, a strain gradient naturally exists around the dislocation cores and can significantly influence the electrical and mechanical properties. We use aberration corrected scanning transmission electron microscopy to directly measure the flexoelectric polarization ( $\sim 28 \mu\text{C cm}^{-2}$ ) at dislocation cores in SrTiO<sub>3</sub>. The polarization charges can interact with the nonstoichiometric dislocation cores and thus impact the electrical activities. Our findings can help us to understand the properties of dislocations in perovskite, providing new insights into the design of new devices via defect engineering such as bicrystal fabrication and thin film growth.

DOI: [10.1103/PhysRevLett.120.267601](https://doi.org/10.1103/PhysRevLett.120.267601)

Crystalline materials usually contain dislocations and grain boundaries which, reportedly, exhibit a very different nature from the rest of the bulk matrix [1–9]. The presence of these defects can significantly influence properties such as ionic and electrical conductivities or can even dominate the entire response in nanoscale devices [8–10]. For instance, the dislocations in antiferromagnetic NiO are indeed ferromagnetic [9], while the grain boundary of ferromagnetic La<sub>2/3</sub>Ca<sub>1/3</sub>MnO<sub>3</sub> becomes paramagnetic [11]. In electroceramics such as SrTiO<sub>3</sub> (STO, a representative perovskite oxide), the dislocations and grain boundaries are generally considered to be charged largely due to nonstoichiometry [12,13], which may account for the unique electrical and ionic transport properties [14–17]. In fact, besides the possible nonstoichiometry in these defects, the occurrence of strain is also inevitable due to an altered continuity in the atomic bonding. Moreover, because of the strong coupling between lattice and charge (i.e., the electromechanical effects) in these oxides, the presence of strain at the defects is also believed to impact the electrical activity via the piezoelectricity and/or flexoelectricity.

The flexoelectricity is, actually, the strain gradient induced electric dipole moments [18], being a property of all insulators, and it can considerably influence the functionalities of materials, particularly for high permittivity materials that have a large flexoelectric coefficient, such as STO and BaTiO<sub>3</sub>. For instance, both theoretical and experimental investigations have shown that the mechanical response of ferroelectrics to inhomogeneous strain

depends on the polarization orientation because of the flexoelectric effect [19,20]. Although the ideal STO is not a ferroelectric material, the flexoelectric effect induced polarization has been predicted around the dislocations even at room temperature [21], and localized electric dipoles have also been theoretically calculated [22]. These dipoles are expected to induce bound charge accumulation at the defects due to the broken continuity of dipole moments [23,24]. The bound charge further requires compensation or screening from either external or internal aspects, e.g., surface absorption, free carrier redistribution, and accumulation of point defects such as oxygen vacancies [23,24]. In this scenario, the electrical activity of polarized dislocations and grain boundaries in electroceramics might be significantly different from conventional assumptions. Nevertheless, in the well-established macroscopic electroceramic theory, whether or not a polarized phase exists at the dislocation cores and grain boundaries in STO is rarely discussed, and how it influences the electrical activity remains largely unknown.

Here, we directly observe stable localized electric dipoles exist near the dislocation cores in a 10° small tilt grain boundary of STO bicrystal ((001)/[100]) at room temperature. Formation of such a stable polarized zone results from strain gradient induced flexoelectricity. Strong interaction subsequently takes place between the polarization bound charge and nonstoichiometric dislocation cores (via polarization screening), leading to huge octahedral distortions and significant charge redistribution at the

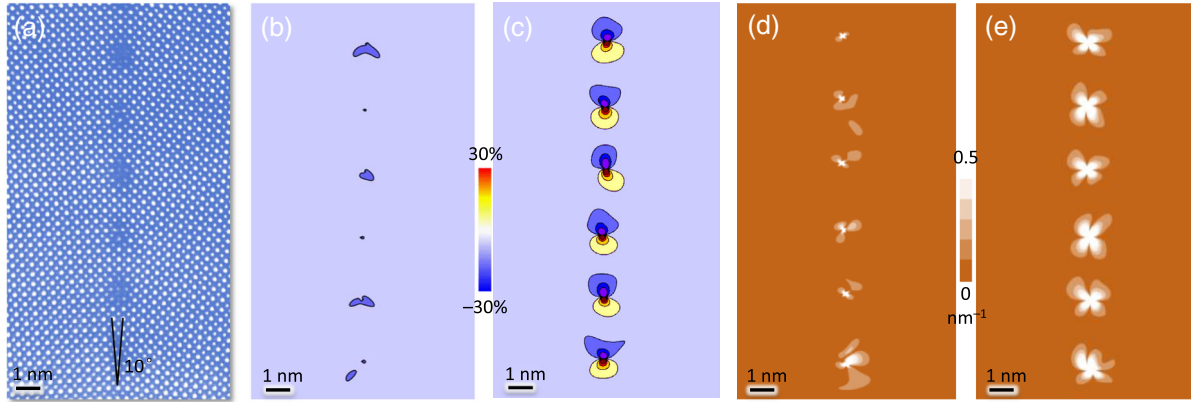


FIG. 1. Strain distribution at a  $10^\circ$  SrTiO<sub>3</sub> grain boundary. (a) HAADF image. GPA showing strain distributions (b)  $e_{xx}$  nearly parallel to the grain boundary plane and (c)  $e_{zz}$  nearly perpendicular to the grain boundary plane. Calculated strength of strain gradients from (d)  $e_{xx}$  and (e)  $e_{zz}$ .

defects. Since the polarization charge in the dipole zone is of the same order of undercoordination number of non-stoichiometric defects, the screening mechanism involving charge redistribution is expected to reasonably influence the electrical activities. The presence of localized stable dipole moments can help us to explain the electrical and ionic transport properties of dislocations and grain boundaries in electroceramic STO.

A high angle annular dark field (HAADF) of the scanning transmission electron microscopy (STEM) image in Fig. 1(a) shows that a  $10^\circ$  grain boundary in STO bicrystal consists of two alternate dislocation cores [14]. The experiment details are included in the Supplemental Material [25]. Although these dislocations have the same Burgers vector of  $\mathbf{a}[100]$ , their atomic structure is different; i.e., the *A*-type dislocation core is SrO plane terminated while the *B*-type dislocation core is TiO<sub>2</sub> terminated [26]. The geometric phase analysis (GPA) [27,28] in Figs. 1(a)–1(d) (see Fig. 1 in the Supplemental Material [25] for further details) indicates that the strain is as high as 10% within the first two unit cells from the grain boundary plane, which is consistent with the simultaneously recorded low-angle ADF image (that is, sensitive to the stain field) shown in Fig. 2 of the Supplemental Material [25]. By comparing Figs. 1(b) and 1(c), we find that the strain field is inhomogeneous and mainly along the direction perpendicular to the grain boundary plane. The calculated lateral strain gradient is at the level of  $\sim 0.1\text{--}1\text{ nm}^{-1}$  within the first two unit cells at the dislocation cores. Considering the flexoelectric effect stem from the strain gradient, we therefore expect electric dipoles to exist near the dislocation.

To provide direct evidence whether or not there is strain gradient induced flexoelectric polarization at the microscopic length scale, we performed a piezoelectric force microscopy (PFM) measurement [29,30] in the grain boundary region [31]. The topography at the grain boundary in Fig. 2(a) shows no distinguishable features of surface compared to the other regions, indicating a

smooth surface and the high quality nature of the boundary, which is consistent with the STEM results. The experimental configuration for the in-plane PFM measurement is shown in Fig. 2(b), in which the tip is along the boundary and is thus sensitive to the piezoresponse perpendicular to the boundary plane. To avoid the disturbance of the topography, trace [Fig. 2(c)] and retrace [Fig. 2(d)] signals are collected at the same time. On both sides of the grain boundary, the in-plane PFM images show the piezoresponse contrast, confirming the presence of electric dipoles at the grain boundary. The opposite piezoresponse responses (the blue and brown regions) at the two sides of

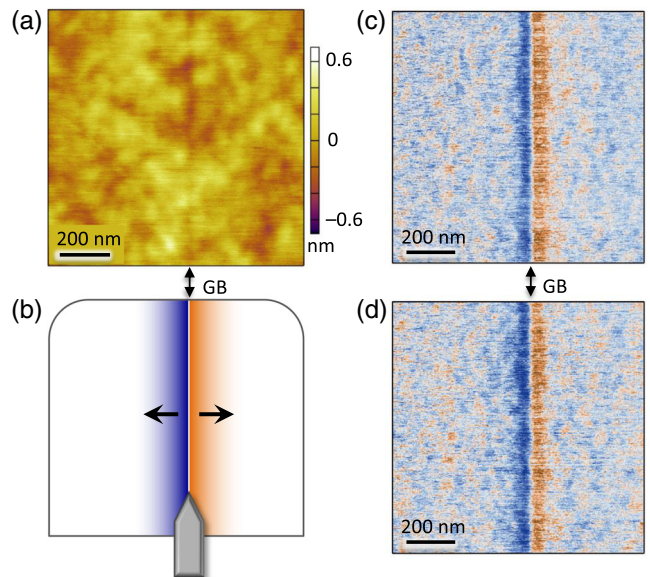


FIG. 2. PFM measurement. (a) Topography. (b) Schematic illustration showing the electric dipole component perpendicular to the grain boundary plane. In-plane PFM measurements from (c) a left-to-right scan (trace) and (d) a right-to-left scan (retrace), respectively. The measured signal is amplitude  $\times \cos$  (phase).

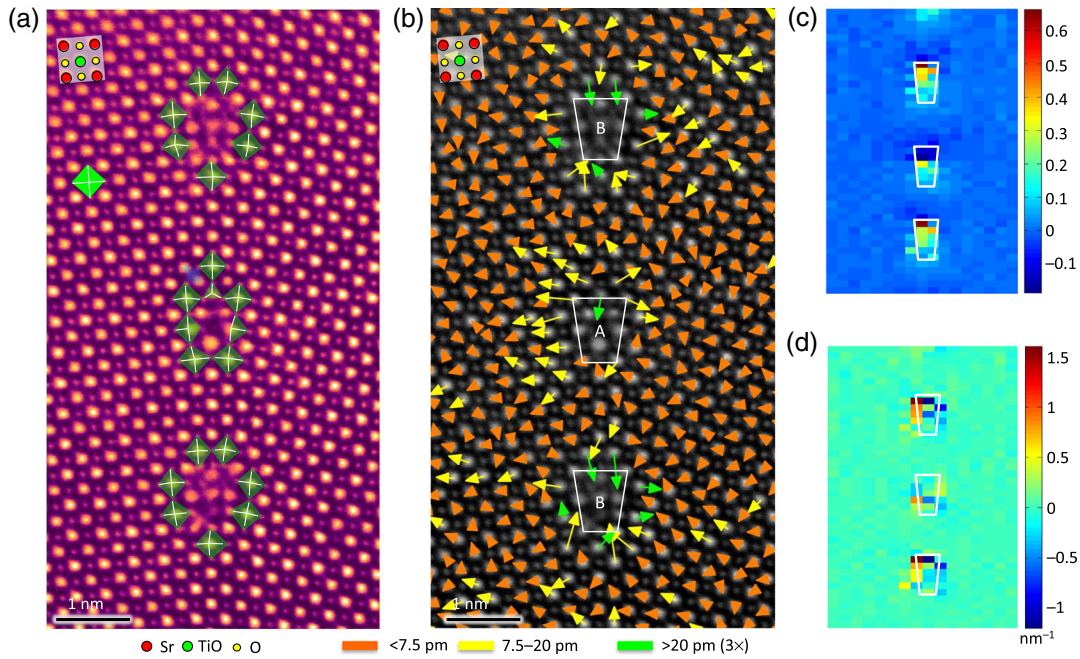


FIG. 3. Polarization at the dislocations in  $\text{SrTiO}_3$ . (a) Near the dislocation cores, oxygen octahedron distortion is visible with the naked eye. The contrast of the ABF image is inverted and colored for clarity. (b) The vector map of displacement between the Sr and TiO columns. Orange vectors,  $<7.5$  pm; yellow,  $7.5\text{--}20$  pm; green,  $>20$  pm ( $3\times$ ). The unit cell scale mapping of (c) strain and (d) the corresponding strain gradient perpendicular to the grain boundary plane. The dislocation cores are highlighted by the white trapezoids.

the grain boundary suggest tail-to-tail polarization across the grain boundary, as schematically illustrated by the black arrows in Fig. 2(b). In fact, a previous PFM characterization of a STO polycrystal also showed enhanced piezoresponse signal at the grain boundary [31], which was proposed to be due to the presence of dipole moments. However, it should be noted that the possible space charges at the dislocations can also contribute to the PFM measurement [29,30]. By contrast, it was reported that a quantitative image analysis and electron energy loss spectroscopy (EELS) in STEM [32,33] could effectively decouple these effects. In the following, these techniques are used to characterize the dislocations.

In Fig. 3(a), within the first unit cell of the dislocation cores, the octahedral distortion is large enough to be recognizable in the contrast inverted annular bright field (ABF) image (see also Fig. 3 of the Supplemental Material [25]). For example, the TiO column highlighted by the white arrow shifts away from the core A to form an oxygen pyramid, instead of octahedral configuration, in this trapezoid-shaped unit cell. The strength of polarization can be calculated from the quantitative image analysis [34,35] via a measurement of atomic displacements. However, the atomic displacements between cations and oxygen are too sensitive to specimen tilt [35], which is evitable at the grain boundary of the bicrystal. Therefore, the displacement vector of the relative off centering between Sr and the neighboring TiO columns [36] with minimized tilt effect [35] is measured to estimate the polarization in Fig. 3. The nonzero displacement is only

expected in a polarized domain, and it represents spontaneous polarization [34,36],  $P_s \propto \Delta z$ , where  $P_s$  is the spontaneous polarization and  $\Delta z$  is the magnitude of the displacement. In the left and right sides of the dislocations in Fig. 3(b), the yellow and green displacement vectors are well above the noise level (see Fig. 4 in the Supplemental Material [25]), and those around core A point away from the grain boundary. The orientation of displacement vectors is consistent with the strain gradient direction in Fig. 1.

At the dislocation core A, with all of the electric dipoles pointing towards radial direction, the dislocation core is negatively poled due to the tail-to-tail configuration of the electric dipoles, which is identical to the “charged domain wall” in ferroelectrics [37,38]. Given the mean value of  $\sim 11$  pm for the yellow displacement vectors around the core A, the spontaneous polarization is estimated to be  $\sim 28 \mu\text{C cm}^{-2}$  (Ref. [36], equivalent to  $1.8 \times 10^{14} e \text{ cm}^{-2}$ ), where  $e$  is the elementary charge. The strain and strain gradient is also mapped at the atomic scale based on the cation sublattice measurements in Figs. 3(c) and 3(d) (see the experimental section and Fig. 5 in the Supplemental Material [25]). Within the first two unit cells, the strain gradient is up to  $\sim 0.1\text{--}1 \text{ nm}^{-1}$ . Therefore, the flexoelectric coefficient is estimated to be  $\sim 0.3\text{--}3 \text{ nC m}^{-1}$ , which is in good agreement with the reported value [21].

However, at the dislocation core B, the atomic displacements have no simple correspondence to the polarization due to the presence of nonperovskite structure and cationic point defects (e.g., Sr vacancies, Ti-antisite defects) in the core

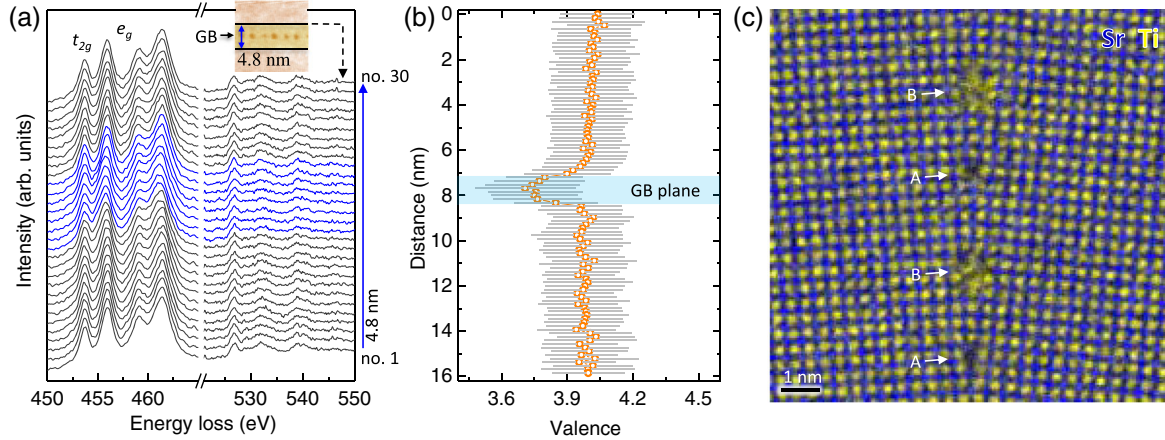


FIG. 4. Electronic structures and elemental distribution in  $\text{SrTiO}_3$  dislocations. (a) The Ti-L edges across the grain boundary. The blue spectra are from the grain boundary plane. (Inset) The recorded spectra region. (b) The plot of the average Ti valence across the grain boundary plane. (c) Atomically resolved EDS measurement.

region, which was confirmed by the energy-dispersive x-ray spectroscopy (EDS) mapping in a previous work [26], and below as well. These cationic defects can provide high-density nanometer-size polar clusters (NPCs), from which the ferroelectricity in STO was believed to originate [39,40]. Previous first-principles calculations [41] showed that Ti-antisite induced polarization is as large as  $55 \mu\text{C}/\text{cm}^2$  in its residing unit cell and also causes other surrounding region to be coherently polarized. These NPCs can be aligned by the dislocation–grain boundary generated strain fields [42] to form net electric dipole moments. Furthermore, in the grain boundary plane [Fig. 3(b)] around the dislocation core B, the orientation of displacement vectors between the tensile and compressive regions is opposing, which further confirms that the atomic displacements are driven by the strain gradient. It should be noted that the measured polarization is not purely from flexoelectricity because, within the first two unit cells of these dislocations, the strain itself is large enough [Figs. 1(b) and 1(d)] to cause a phase transition from paraelectric to ferroelectric STO [43]. However, unlike the thin film structure, the strain changes dramatically around the dislocations, and thus the flexoelectric effect induced polarization likely dominates.

At the physical boundaries, the broken continuity of electric dipoles causes the immobile polarization charge accumulation. These bound charges must be screened by either free carriers or charged defects; otherwise, the electric dipoles become unstable. For example, at the core A, the tail-to-tail configuration of the electric dipoles has a negative bound charge which must be screened by the positive charges at the grain boundary cores. In order to investigate the screening mechanism of flexoelectric polarization, the EELS measurements of the electronic structures of the dislocations were carried out and are shown in Fig. 4(a) (see Fig. 6 in the Supplemental Material [25] for further details), in which the Ti-L edges at the grain boundary shift to the lower energy and have a less

pronounced peak splitting of  $t_{2g}$  and  $e_g$  and the peaks in the O-K edges become flat, suggesting reduced Ti and the presence of oxygen vacancies. By fitting the Ti-L edges with the reference  $\text{Ti}^{4+}$  (from bulk  $\text{SrTiO}_3$ ) and  $\text{Ti}^{3+}$  (from bulk  $\text{LaTiO}_3$ ) spectra in Fig. 4(b), the reduced Ti ions are mainly concentrated near the grain boundary plane, where the calculated valence of Ti is as low as  $\sim 3.5+$  [26]. Besides the anionic point defects, complex cationic point defects also exist in the dislocation cores [26] from the atomically resolved EDS measurement in Fig. 4(c). Sr vacancies exist in the core B, and Ti unexpectedly appears in some Sr columns (Ti antisites) [26]. These cationic defects can generate NPCs [41]. On the other hand, the charged point defects in the grain boundary plane could also act as the screening charge to interact with the flexoelectric dipole moments [39,40].

Assuming that the flexoelectric effect induced polarization bound charge at the dislocation core is completely screened by these charged defects, it requires about  $0.3 e$  charge (e.g., 0.15 O vacancies) in each unit cell. This is at the same level of nonstoichiometry as the EELS measurements in Fig. 4(b), indicating that the screening mechanism of flexoelectric electric dipoles is as important as the nonstoichiometry in determining the electrical activities of dislocations and grain boundaries. For example, along an oxygen vacancy-rich dislocation core or grain boundary, whether oxygen ionic conductivity is enhanced [44] or impeded [45] is a long-standing debate. Recently, Marrocchelli *et al.* clarified that, although the concentration of oxygen vacancies at the dislocation cores is higher, oxygen transport along the dislocation is actually slower [46] due to the higher barrier to diffuse. The strong interaction between the flexoelectric polarization and the charged point defects in the nonstoichiometric grain boundary may account for the high ionic diffusion barrier: despite high density of oxygen vacancies at the grain boundary, most of them are effectively “pinned” by the

flexoelectric electric dipoles via a polarization bound charge screening mechanism. The transport properties across the grain boundary plane consisting of such dislocation arrays can also be affected by the presence of electric dipoles, which drives the positive charge (e.g., oxygen vacancies or holes) and electrons spatially separated to screen the depolarizing fields, forming a depleted zone. Such a scenario brings new insight into the well-known double Schottky barrier model for a low-angle grain boundary [12] and thus should influence electrical and ionic conductivities (see Refs. [45,46] and references therein) in a complicated manner.

In summary, we identify in this Letter that a localized stable polarized zone exists at the dislocation cores in a 10° STO grain boundary. The point defects, strain field and strain gradient, and nonstoichiometry account for the stable electric dipoles. Our results suggest that the localized polarized zone plays an important role in determining the electrical activities of dislocations and low-angle grain boundaries, as flexoelectric polarization induced bound charge must be screened via a redistribution of free carriers or charged defects. The new insights provided by the localized polarized dislocations can help us to explain some of the past studies, such as the high ionic diffusion barrier along the dislocation cores, and also add more information about the double Schottky barrier model for the low-angle grain boundary in electroceramic STO.

Part of this study was supported by a Grant-in-Aid for Specially Promoted Research (Grant No. JP17H06094) and a Grant-in-Aid for Scientific Research on Innovative Areas “Nano Informatics” from the Japan Society for the Promotion of Science (JSPS), a Grant-in-Aid for Scientific Research on Innovative Areas “Nano Informatics” (Grant No. 25106003) from JSPS, and the “Nanotechnology Platform” (Project No. 12024046) from the Ministry of Education, Culture, Sports, Science and Technology in Japan (MEXT). P. G. received support from a Japan Society for the Promotion of Science (JSPS) fellowship for part of this work. P. G. acknowledges support from the National Key R&D Program of China (Grants No. 2016YFA0300804 and No. 2016YFA0300903), the National Natural Science Foundation of China (Grants No. 51672007, No. 51502007, and No. 11327902), National Equipment Program of China (ZDYZ2015-1), the National Program for Thousand Young Talents of China, and the “2011 Program” Peking-Tsinghua-IOP Collaborative Innovation Center for Quantum Matter. The work at Tsinghua was supported by the National Basic Research Program of China (Grants No. 2015CB921700 and No. 2016YFA0301004); and the Beijing Advanced Innovation Center for Future Chip (ICFC).

\*p-gao@pku.edu.cn

†ikuhara@sigma.t.u-tokyo.ac.jp

‡These authors contributed equally to this work.

- [1] M. M. McGibbon, N. D. Browning, M. F. Chisholm, A. J. McGibbon, S. J. Pennycook, V. Ravikumar, and V. P. Dravid, *Science* **266**, 102 (1994).
- [2] M. Kim, G. Duscher, N. D. Browning, K. Sohlberg, S. T. Pantelides, and S. J. Pennycook, *Phys. Rev. Lett.* **86**, 4056 (2001).
- [3] J. P. Buban, K. Matsunaga, J. Chen, N. Shibata, W. Y. Ching, T. Yamamoto, and Y. Ikuhara, *Science* **311**, 212 (2006).
- [4] N. Shibata, M. F. Chisholm, A. Nakamura, S. J. Pennycook, T. Yamamoto, and Y. Ikuhara, *Science* **316**, 82 (2007).
- [5] N. Shibata, S. D. Findlay, S. Azuma, T. Mizoguchi, T. Yamamoto, and Y. Ikuhara, *Nat. Mater.* **8**, 654 (2009).
- [6] Y. Ikuhara, *Prog. Mater. Sci.* **54**, 770 (2009).
- [7] Y. L. Tang, Y. L. Zhu, Y. Liu, Y. J. Wang, and X. L. Ma, *Nat. Commun.* **8**, 15994 (2017).
- [8] K. Szot, W. Speier, G. Bihlmayer, and R. Waser, *Nat. Mater.* **5**, 312 (2006).
- [9] I. Sugiyama, N. Shibata, Z. Wang, S. Kobayashi, T. Yamamoto, and Y. Ikuhara, *Nat. Nanotechnol.* **8**, 266 (2013).
- [10] D. M. Marincel *et al.*, *Phys. Rev. B* **91**, 134113 (2015).
- [11] R. Gross *et al.*, *J. Magn. Magn. Mater.* **211**, 150 (2000).
- [12] Y. M. Chiang and T. Takagi, *J. Am. Ceram. Soc.* **73**, 3278 (1990).
- [13] R. Waser, *Solid State Ionics* **75**, 89 (1995).
- [14] Z. Zhang, W. Sigle, and M. Rühle, *Phys. Rev. B* **66**, 094108 (2002).
- [15] S. Y. Choi, J. P. Buban, M. Nishi, H. Kageyama, N. Shibata, T. Yamamoto, S. J. L. Kang, and Y. Ikuhara, *J. Mater. Sci.* **41**, 2621 (2006).
- [16] J. P. Buban, M. Chi, D. J. Masiel, J. P. Bradley, B. Jiang, H. Stahlberg, and N. D. Browning, *J. Mater. Res.* **24**, 2191 (2009).
- [17] H. Du, C.-L. Jia, L. Houben, V. Metlenko, R. A. De Souza, R. Waser, and J. Mayer, *Acta Mater.* **89**, 344 (2015).
- [18] P. Zubko, G. Catalan, and A. K. Tagantsev, *Annu. Rev. Mater. Res.* **43**, 387 (2013).
- [19] A. Abdollahi, C. Peco, D. Millan, M. Arroyo, G. Catalan, and I. Arias, *Phys. Rev. B* **92**, 094101 (2015).
- [20] K. Cordero-Edwards, N. Domingo, A. Abdollahi, J. Sort, and G. Catalan, *Adv. Mater.* **29**, 1702210 (2017).
- [21] P. Zubko, G. Catalan, A. Buckley, P. R. L. Welche, and J. F. Scott, *Phys. Rev. Lett.* **99**, 167601 (2007).
- [22] P. Hirel, M. Mrovec, and C. Elsaesser, *Acta Mater.* **60**, 329 (2012).
- [23] P. Gao *et al.*, *Nat. Commun.* **8**, 15549 (2017).
- [24] P. Gao, H.-J. Liu, Y.-L. Huang, Y.-H. Chu, R. Ishikawa, B. Feng, Y. Jiang, N. Shibata, E.-G. Wang, and Y. Ikuhara, *Nat. Commun.* **7**, 11318 (2016).
- [25] See Supplemental Material at <http://link.aps.org/supplemental/10.1103/PhysRevLett.120.267601> for a discussion of the bicrystal fabrication, the HAADF and ABF image acquisition and analysis, the EDS experiment, the EELS experiment, the PFM measurement, the geometric phase analysis, additional evidence of strain near the dislocation cores, the ABF image, the noise evaluation, and the calculation of lattice parameters, and for additional information on the EELS characterization.
- [26] P. Gao, R. Ishikawa, B. Feng, A. Kumamoto, N. Shibata, and Y. Ikuhara, *Ultramicroscopy* **184**, 217 (2018).

- [27] The geometric phase analysis DigitalMicrograph plug-in, developed by Kotch *et al.*, is available at <https://www.physics.hu-berlin.de/en/sem>.
- [28] M. J. Hytch, E. Snoeck, and R. Kilaas, *Ultramicroscopy* **74**, 131 (1998).
- [29] N. Balke, I. Bdikin, S. V. Kalinin, and A. L. Kholkin, *J. Am. Ceram. Soc.* **92**, 1629 (2009).
- [30] S. V. Kalinin, A. N. Morozovska, L. Q. Chen, and B. J. Rodriguez, *Rep. Prog. Phys.* **73**, 056502 (2010).
- [31] A. Kholkin, I. Bdikin, T. Ostapchuk, and J. Petzelt, *Appl. Phys. Lett.* **93**, 222905 (2008).
- [32] Y. M. Kim, J. He, M. D. Biegalski, H. Ambaye, V. Lauter, H. M. Christen, S. T. Pantelides, S. J. Pennycook, S. V. Kalinin, and A. Y. Borisevich, *Nat. Mater.* **11**, 888 (2012).
- [33] Y.-M. Kim, A. Morozovska, E. Eliseev, M. P. Oxley, R. Mishra, S. M. Selbach, T. Grande, S. T. Pantelides, S. V. Kalinin, and A. Y. Borisevich, *Nat. Mater.* **13**, 1019 (2014).
- [34] C. T. Nelson *et al.*, *Nano Lett.* **11**, 828 (2011).
- [35] P. Gao, A. Kumamoto, R. Ishikawa, N. Lugg, N. Shibata, and Y. Ikuhara, *Ultramicroscopy* **184**, 177 (2018).
- [36] S. C. Abrahams, S. K. Kurtz, and P. B. Jamieson, *Phys. Rev.* **172**, 551 (1968).
- [37] P. Gao, J. Britson, J. R. Jokisaari, C. T. Nelson, S.-H. Baek, Y. Wang, C.-B. Eom, L.-Q. Chen, and X. Pan, *Nat. Commun.* **4**, 2791 (2013).
- [38] T. Sluka, A. K. Tagantsev, P. Bednyakov, and N. Setter, *Nat. Commun.* **4**, 1808 (2013).
- [39] G. Burns and F. H. Dacol, *Phys. Rev. B* **28**, 2527 (1983).
- [40] L. E. Cross, *Ferroelectrics* **76**, 241 (1987).
- [41] D. Lee *et al.*, *Science* **349**, 1314 (2015).
- [42] H. W. Jang *et al.*, *Phys. Rev. Lett.* **104**, 197601 (2010).
- [43] J. H. Haeni *et al.*, *Nature (London)* **430**, 758 (2004).
- [44] K. Szot, W. Speier, R. Carius, U. Zastrow, and W. Beyer, *Phys. Rev. Lett.* **88**, 075508 (2002).
- [45] V. Metlenko, A. H. Ramadan, F. Gunkel, H. Du, H. Schraknepper, S. Hoffmann-Eifert, R. Dittmann, R. Waser, and R. A. De Souza, *Nanoscale* **6**, 12864 (2014).
- [46] D. Marrocchelli, L. Sun, and B. Yildiz, *J. Am. Chem. Soc.* **137**, 4735 (2015).